

ADAPTIVE PRACTICAL PRESCRIBED-TIME FAULT-TOLERANT CONTROL FOR SMALL TANDEM-ROTOR UAV FORMATIONS

Xiaolu Li[1], Changqing Wang[1], Yong Guo[1], & Aijun Li[1]

[1]School of Automation, Northwestern Polytechnical University, Xi'an, 710129, China

Abstract

This paper proposes an adaptive distributed prescribed-time fault-tolerant control strategy for small tandem-rotor UAV (STR-UAV) formations subject to external disturbances and actuator effectiveness faults. A prescribed-time sliding mode surface is designed to guarantee formation error convergence within a predefined time independent of initial states. A prescribed-time adaptive law is developed to simultaneously estimate unknown disturbances and faults without prior bound information. Rigorous Lyapunov analysis proves closed-loop prescribed-time stability, and numerical simulations verify the strategy's superior convergence speed, disturbance rejection, and fault tolerance.

Keywords: STR-UAV, practical prescribed-time stability, fault-tolerant control, sliding mode surface, adaptive law

1. Introduction

Rotorcraft unmanned aerial vehicles (UAVs) have been widely applied in industrial inspection, agricultural plant protection, military reconnaissance, disaster search and rescue, and other fields due to their remarkable advantages of vertical take-off and landing (VTOL), stable hovering, and high maneuverability [1]. Particularly in post-disaster search and rescue scenarios, rotorcraft UAVs can be rapidly deployed to penetrate hazardous areas inaccessible to humans, performing critical tasks such as life detection, environmental reconnaissance, and information relay, thus becoming one of the core platforms for improving emergency response efficiency [2]. However, the application of traditional multi-rotor UAVs in complex and confined environments still faces numerous challenges [3]: on the one hand, conventional quadrotor UAVs have a relatively wide fuselage, making it difficult to traverse confined spaces such as building ruins, pipes, and tunnels; on the other hand, their limited endurance cannot support large-area, long-duration continuous search missions. To address the above issues, a small tandem-rotor Unmanned Aerial Vehicle (STR-UAV) [4],[5],[6] has attracted increasing attention from the academic community. Compared with traditional quadrotor UAVs, the STR-UAV adopts a layout with two rotors arranged longitudinally along the fuselage axis, which significantly reduces the lateral width of the fuselage and enables it to flexibly enter narrow spaces to perform tasks. In addition, its integrated wheeled mobile mechanism allows it to land safely and traverse ground or vertical surfaces in emergency situations, remarkably enhancing its survivability and mission adaptability in complex unstructured environments.

Although the STR-UAV demonstrates unique advantages in single-platform performance, the endurance and operational range of an individual UAV are still limited by battery capacity, making it difficult to independently complete search missions over large areas [7]. Formation cooperative control, through the collaborative operation of multiple UAVs, can achieve parallel coverage and optimal resource allocation of mission areas, effectively improving search efficiency and mission completion rate. It is therefore a key approach to solving the single-platform capability bottleneck [8],[9]. Consequently, research on formation cooperative control methods for STR-UAVs has important theoretical significance and engineering value.

Among the numerous performance metrics of formation control, convergence time is the core indicator that determines mission timeliness. Traditional control methods based on asymptotic stability theory [10] cannot guarantee finite-time system convergence, making it difficult to meet the strict response

speed requirements of practical missions. Although finite-time [11] and fixed-time [12] control theories can achieve finite/fixed-time convergence, the convergence time upper bound of the former depends on the system initial states, while the convergence time of the latter cannot be predefined according to mission requirements. Both are difficult to adapt to search and rescue missions with explicit time constraints. In contrast, prescribed-time control theory [13] enables the strict upper bound of system convergence time to be predefined according to mission requirements, and this upper bound is independent of the system initial states and control parameters. It can provide predictable time performance guarantees for formation control and has become a topic of intense current research in the field of formation control.

In addition, STR-UAV formations face complex uncertainties and fault threats during actual flight. On the one hand, external environmental disturbances such as atmospheric turbulence and gusts directly affect the flight attitude and position accuracy of UAVs, and may even lead to formation instability [14]. On the other hand, actuator aging, mechanical wear, or sudden damage may cause actuator faults, resulting in degradation of control effectiveness, which in severe cases may lead to mission failure or even UAV destruction [15]. To address these problems, domestic and foreign scholars have proposed various solutions: robust control methods such as sliding mode control [16] and active disturbance rejection control [17] suppress disturbance effects by designing robust control laws; estimation methods such as adaptive laws [18] and disturbance observers [19] improve system performance by estimating and compensating for disturbances in real time; intelligent control methods such as deep learning [20] and reinforcement learning [21] achieve adaptive control in complex environments through data-driven approaches. However, robust control methods usually suffer from high conservatism, while intelligent control methods impose an enormous computational burden and cannot easily guarantee closed-loop stability. In comparison, adaptive control methods can perform online estimation of unknown disturbances and fault parameters without prior knowledge of their upper bounds, achieving a good balance among control accuracy, computational complexity, and engineering practicability. They provide an efficient technical approach for solving disturbance rejection and fault-tolerant control problems in formation control.

In summary, this paper proposes a practical prescribed-time formation fault-tolerant control strategy to address the convergence time constraints, external disturbances, and actuator faults faced by STR-UAV formations when performing search missions in complex environments. This strategy ensures the prescribed-time convergence performance of the system by designing a prescribed-time sliding mode surface, and simultaneously achieves online estimation and compensation of external disturbances and actuator faults by combining a prescribed-time adaptive law. The main contributions of this paper are as follows:

(1) A prescribed-time sliding mode surface is proposed to address the strict temporal convergence requirement in formation control. Compared with conventional finite-time and fixed-time sliding mode surfaces, the proposed design allows the convergence time upper bound to be explicitly predefined according to practical engineering requirements, and crucially, this bound is completely independent of the system's initial states. Rigorous theoretical analysis guarantees that the system states converge to the sliding mode surface within the specified time interval.

(2) A prescribed-time adaptive law is developed for accurate estimation of unknown external disturbances. Unlike traditional adaptive laws that only ensure asymptotic convergence of estimation errors, the proposed adaptive law achieves prescribed-time convergence of disturbance estimation errors, enabling rapid and precise compensation for time-varying environmental perturbations.

(3) An integrated adaptive prescribed-time formation fault-tolerant control strategy is constructed by combining the aforementioned sliding mode surface and adaptive law. This strategy simultaneously achieves three critical objectives: prescribed-time stability of the entire STR-UAV formation system, effective suppression of external atmospheric disturbances, and active accommodation of actuator effectiveness faults. It significantly enhances the robustness and mission reliability of STR-UAV formations operating in complex unstructured environments.

2. Prerequisites and Formation Model

2.1 Prerequisites

For a differential system

$$\dot{\boldsymbol{x}}(t) = f(\boldsymbol{x}, t), \boldsymbol{x}(0) = \boldsymbol{x}_0 \tag{1}$$

where $\boldsymbol{x}(t) \in R^n$ represents the system state.

Definition 1 The definitions of prescribed-time stability and practical prescribed-time stability are as follows:

(1) The system is said to be prescribed-time stable if it is asymptotically stable, and there exists a time $T_p > 0$ such that $T(\boldsymbol{x}_0) \le T_p$ holds for all initial states, where $\|\boldsymbol{x}(\boldsymbol{x}_0, t)\| = 0$ for all $t \ge T(\boldsymbol{x}_0)$. Here, T_p is a parameter that is independent of the initial states of the system and can be arbitrarily selected according to task requirements.

(2) The system is said to be prescribed-time stable if it is asymptotically stable, and there exists a time $T_p > 0$ such that $T(\boldsymbol{x}_0) \le T_p$ holds for all initial states, where $\|\boldsymbol{x}(\boldsymbol{x}_0, t)\| \le \rho$ for all $t \ge T(\boldsymbol{x}_0)$. Here, T_p is a parameter that is independent of the initial states of the system and can be arbitrarily selected according to task requirements.

Lemma 1 [13] For system (1), if there exists a Lyapunov function satisfying the inequality shown in Eq. (2), then system (1) is prescribed-time stable.

$$\dot{V}(\boldsymbol{x}) \le -c\vartheta(t)V(\boldsymbol{x}) + \varepsilon \tag{2}$$

where $c > 0$ and $\varepsilon > 0$ are positive constants. The function $\vartheta(t)$ and its first-order derivative are given by Eq. (3) and Eq. (4), respectively.

$$\vartheta(t) = \begin{cases} \dfrac{1}{\gamma}\left(1 - e^{-\frac{\varphi t}{T-t}}\right), & if\ t < T \\ \dfrac{1}{\gamma}, & if\ t \ge T \end{cases} \tag{3}$$

$$\dot{\vartheta}(t) = \begin{cases} \dfrac{\varphi T}{\gamma (T-t)^2} e^{-\frac{\varphi t}{T-t}}, & if\ t < T \\ 0, & if\ t \ge T \end{cases} \tag{4}$$

where $\gamma \in (0,1)$ and $\varphi \in (0,1)$. $T > 0$ denotes the prescribed-time parameter. That is, the system state vector $\boldsymbol{x}$ will converge to the set $\mathrm{E} = \max\{\mathrm{E}_1, \mathrm{E}_2\}$ within the prescribed time T.

$$\mathrm{E}_1 = \left\{ \boldsymbol{x} : V(\boldsymbol{x}) \le V(0) e^{-\frac{cT\varphi}{\gamma(1+\varphi)}} + \frac{\varepsilon\gamma T/(c\varphi)}{\sqrt{T^2/4 + \gamma T/(c\varphi)}} \ln\left(\frac{\sqrt{T^2/4 + \gamma T/(c\varphi)} + T/2}{\sqrt{T^2/4 + \gamma T/(c\varphi)} - T/2} \right) \right\} \tag{5}$$

$$\mathrm{E}_2 = \left\{ \boldsymbol{x} : V(\boldsymbol{x}) \le \frac{\gamma\varepsilon}{c} + \left(V\left(\boldsymbol{x}(T)\right) - \frac{\gamma\varepsilon}{c} \right) e^{-\frac{c}{\gamma}(t-T)} \right\} \tag{6}$$

2.2 Formation Model

Considering a distributed STR-UAV formation consisting of one leader and m followers. The model for the i th follower can be expressed as:

$$\begin{cases} \dot{p}_{ix} = V_i \cos\theta_i \cos\psi_i \\ \dot{p}_{iy} = V_i \cos\theta_i \sin\psi_i \\ \dot{p}_{iz} = V_i \sin\theta_i \\ \dot{V}_i = \dfrac{T_i - D_i + d_{Vi}}{m_i} - g\sin\theta_i \\ \dot{\theta}_i = \dfrac{L_i \cos\phi_i - m_i g \cos\theta_i + d_{\theta i}}{m_i V_i} \\ \dot{\psi}_i = \dfrac{L_i \sin\phi_i + d_{\psi i}}{m_i V_i \cos\theta_i} \end{cases} \tag{7}$$

where the subscript i indexes the i th STR-UAV. p_{ix}, p_{iy}, and p_{iz} correspond to the three-dimensional spatial coordinates measured in the inertial reference frame. V_i, ϕ_i, θ_i, and ψ_i denote

the forward flight velocity, roll angle, track pitch angle and track yaw angle, respectively. L_i, T_i, and D_i represent the aerodynamic lift, thrust and drag forces acting in the body-fixed coordinate system of the aircraft. m_i is the total mass of the UAV, and g stands for the gravitational acceleration constant. d_{Vi}, $d_{\theta i}$, and $d_{\psi i}$ represent the bounded external disturbances acting on each control channel. To facilitate the subsequent controller design procedure, define the following state vectors: $\boldsymbol{p}_i=[p_{ix},p_{iy},p_{iz}]^T$, $\boldsymbol{v}_i=[v_{ix},v_{iy},v_{iz}]^T$, and $\boldsymbol{l}_{is}=[d_{iV},d_{i\theta},d_{i\psi}]^T$. Based on these definitions, the dynamic model of the i th follower UAV can be formulated as follows:

$$\begin{cases}\dot{\boldsymbol{p}}_i=\boldsymbol{v}_i\\ \dot{\boldsymbol{v}}_i=\boldsymbol{w}_i+\boldsymbol{h}_i\left(\boldsymbol{u}_{im}+\boldsymbol{l}_{is}\right)\end{cases} \tag{8}$$

where $\boldsymbol{p}_i$ and $\boldsymbol{v}_i$ represent the position and velocity vectors of the i th UAV expressed in the inertial reference frame respectively. The virtual control input vector is defined as $\boldsymbol{u}_{im}=[T_i,L_i\cos\phi_i,L_i\sin\phi_i]^T$. $\boldsymbol{w}_i=\boldsymbol{W}_i/m_i$ corresponds to the control-input-independent dynamic terms. $\boldsymbol{h}_i=\boldsymbol{H}_i/m_i$ accounts for the control-input-dependent dynamic components.

$$\boldsymbol{H}_i=\begin{bmatrix}\cos\theta_i\cos\psi_i & -\sin\theta_i\cos\psi_i & -\sin\psi_i\\ \cos\theta_i\sin\psi_i & -\sin\theta_i\sin\psi_i & \cos\psi_i\\ \sin\theta_i & \cos\theta_i & 0\end{bmatrix} \tag{9}$$

$$\boldsymbol{W}_i=\begin{bmatrix}-D_i\cos\theta_i\cos\psi_i\\ -D_i\cos\theta_i\sin\psi_i\\ -D_i\sin\theta_i-m_ig\end{bmatrix} \tag{10}$$

Consider the following actuator fault model [6],[12],[15]:

$$\boldsymbol{u}_{im}=\boldsymbol{\omega}_i\boldsymbol{u}_i+\boldsymbol{\eta}_i \tag{11}$$

where $\boldsymbol{\omega}_i=diag(\omega_{ix},\omega_{iy},\omega_{iz})$ denotes the fault coefficient matrix, with each element satisfying $\omega_i\in(0,1]$. $\boldsymbol{\eta}_i=[\eta_{ix},\eta_{iy},\eta_{iz}]^T$ represents the fault bias vector, and $\boldsymbol{u}_i=[u_{ix},u_{iy},u_{iz}]^T$ is the virtual control input signal to be designed. Substituting Eq. (11) into Eq. (8) yields:

$$\begin{cases}\dot{\boldsymbol{p}}_i=\boldsymbol{v}_i\\ \dot{\boldsymbol{v}}_i=\boldsymbol{w}_i+\boldsymbol{h}_i\boldsymbol{u}_i+\boldsymbol{l}_i\end{cases} \tag{12}$$

where $\boldsymbol{l}_i=(\boldsymbol{\omega}_i-\boldsymbol{I}_{3\times3})\boldsymbol{h}_i\boldsymbol{u}_i+\boldsymbol{h}_i(\boldsymbol{\eta}_i+\boldsymbol{l}_{is})$ denotes the lumped error term. Subsequently, the composite formation error for the i th follower STR-UAV is defined as:

$$\tau_{ip}=\sum_{k=1}^{m}\alpha_{ik}\left(\boldsymbol{p}_i-\boldsymbol{p}_k-(\boldsymbol{p}_{id}-\boldsymbol{p}_{kd})\right)+\alpha_{i0}\left(\boldsymbol{p}_i-\boldsymbol{p}_0-\boldsymbol{p}_{id}\right) \tag{13}$$

where $\boldsymbol{p}_{id}=[x_{ixd},x_{iyd},x_{izd}]^T$ denotes the desired relative distance between the leader and the i th follower, $i=1,\cdots,k,\cdots,m$. $\boldsymbol{p}_0=[p_{0x},p_{0y},p_{0z}]^T$ represents the spatial position of the leader.

Assumption 1 The position, velocity and acceleration of the virtual leader are known and continuous.
Assumption 2 The external disturbances and their first-order derivatives, as well as the actuator fault coefficients and fault biases, are unknown but bounded.

3. Main Results

In this section, an adaptive practical prescribed-time fault-tolerant control strategy is constructed by combining a prescribed-time sliding mode surface with a prescribed-time adaptive law.

3.1 Prescribed-time Sliding mode surface

The prescribed-time sliding mode surface is designed as follows:

$$\boldsymbol{s}_i = k_{i2}\dot{\tau}_{ip} + k_{i1}\frac{\cosh^2(\tau_{ip})}{T_{i1}(1-a_i)}\operatorname{sign}\left(\tanh(\tau_{ip})\right)\left|\tanh(\tau_{ip})\right|^{a_i} \tag{14}$$

where $a_i \in (0,1)$, $k_{i1} \geq k_{i2} > 0$ represent the parameters to be designed. while $T_{i1} > 0$ denotes the preset time constant.

Theorem 1 For the system errors (13), when the system states reaches the sliding surface depicted in (14), the formation state error will converge to the origin within a preset time.

Proof: Let $\boldsymbol{s}_i = 0$, then

$$\dot{\tau}_{ip} = -\frac{k_{i1}\cosh^2(\tau_{ip})}{k_{i2}T_{i1}(1-a_i)}\operatorname{sign}\left(\tanh(\tau_{ip})\right)\left|\tanh(\tau_{ip})\right|^{a_i} \tag{15}$$

Construct the Lyapunov function as $V_1 = \left(k_{i2}/k_{i1}\right)\left|\tanh(\tau_{ip})\right|^{1-a_i}$, $V_1 \geq 0$, and differentiate it to obtain:

$$\dot{V}_1 = \frac{k_{i2}(1-a_i)\dot{\tau}_{ip}}{k_{i1}\cosh^2(\tau_{ip})}\operatorname{sign}\left(\tanh(\tau_{ip})\right)\left|\tanh(\tau_{ip})\right|^{-a_i} \tag{16}$$

Substituting (15) into (16) yields:

$$\dot{V}_s = -1/T_{i1} \tag{17}$$

According to the Lyapunov stability theorem, the system is asymptotically convergent. Solving Eq. (17) yields $t \leq V_1(\boldsymbol{x}_0)T_{i1}$, and since $0 \leq V_1 \leq 1$, we have $t \leq T_{i1}$. That is, the proposed sliding mode surface is prescribed-time convergent, with the upper bound of the convergence time being T_{i1}. This completes the proof of Theorem 1.

Remark 1 The prescribed-time sliding mode surface defined by Eq. (15) has its dynamic convergence characteristics determined by four core parameters: the prescribed-time constant T_{i1}, the terminal convergence exponent a_i, and the sliding mode gains k_{i1} and k_{i2}. Specifically, T_{i1} represents the theoretical upper bound for the system errors to converge to the origin, and it is independent of the magnitude of initial errors. A smaller T_{i1} yields faster convergence but causes a sharp increase in control input amplitude, significantly elevating the risk of actuator saturation. Conversely, a larger T_{i1} reduces control energy consumption but results in excessively slow convergence, which fails to meet the real-time requirements of formation systems. The terminal convergence exponent a_i governs the convergence behavior in the small-error neighborhood, which is the essential characteristic that distinguishes terminal sliding mode from conventional linear sliding mode. When $a_i \in (0,1)$, the system exhibits finite-time convergence: a smaller a_i accelerates convergence in the small-error phase but exacerbates control input chattering, while a value closer to 1 mitigates chattering at the cost of reduced convergence speed. Furthermore, the gains k_{i1} and k_{i2} collectively determine the overall convergence rate and control input magnitude, with their ratio k_{i1}/k_{i2} being the dominant factor. A higher ratio enhances both the global convergence speed and robustness against external disturbances, but it also intensifies chattering and increases actuator saturation risk. A lower ratio slows down convergence and slightly degrades robustness, yet it produces smoother control inputs and effectively suppresses chattering. Therefore, the sliding mode surface parameters require a careful trade-off design based on practical application scenarios, aiming to balance system stability, convergence speed, control input constraints, chattering suppression, and robustness.

3.2 Control Strategy Design and Stability Analysis

Taking the derivative of the designed sliding mode surface yields:

$$\dot{\boldsymbol{s}}_i = k_{i2}\left(\sum_{k=0}^{m}\alpha_{ik}\left(\boldsymbol{w}_i + \boldsymbol{h}_i\boldsymbol{u}_i + \boldsymbol{l}_i\right) - \alpha_{i0}\ddot{\boldsymbol{p}}_{id} - \sum_{k=1}^{m}\alpha_{ik}\dot{\boldsymbol{v}}_k\right) + \boldsymbol{\Xi}_i \tag{18}$$

where

$$\boldsymbol{\Xi}_i = \frac{2k_{i1}\cosh(\boldsymbol{\tau}_{ip})\sinh(\boldsymbol{\tau}_{ip})\dot{\boldsymbol{\tau}}_{ip}}{T_{i1}(1-a_i)}\operatorname{sign}\left(\tanh(\tau_{ip})\right)\left|\tanh(\tau_{ip})\right|^{a_i} + \frac{k_{i1}a_i}{T_{i1}(1-a_i)}\operatorname{sign}\left(\tanh(\tau_{ip})\right)\left|\tanh(\tau_{ip})\right|^{a_i-1} \tag{19}$$

Based on this sliding mode surface, the adaptive law and the practical prescribed-time fault-tolerant control strategy is designed as follows:

$$\dot{\hat{\boldsymbol{l}}}_i = \lambda_i k_{i2} \sum_{k=0}^{m} \alpha_{ik} \boldsymbol{s}_i - \frac{1}{2} c_i \vartheta_i \hat{\boldsymbol{l}}_i \tag{20}$$

$$\boldsymbol{u}_i = \boldsymbol{h}_i^{-1} \left[\left(\sum_{k=0}^{m} \alpha_{ik} \right)^{-1} \left(\frac{1}{k_{i2}} \left(-\frac{1}{2} c_i \vartheta_i \boldsymbol{s}_i - \boldsymbol{\Xi}_i \right) + \alpha_{i0} \dot{\boldsymbol{p}}_0 + \sum_{k=1}^{m} \alpha_{ik} \dot{\boldsymbol{v}}_i \right) - \boldsymbol{w}_i - \hat{\boldsymbol{l}}_i \right] \tag{21}$$

where $\lambda_i > 0$ denotes the adaptive gain. Define $\tilde{\boldsymbol{l}}_i = \boldsymbol{l}_i - \hat{\boldsymbol{l}}_i$, where $\hat{l}_i$ and $\tilde{l}_i$ are the estimated value and estimation error of l_i, respectively. Referring to the function ϑ in Lemma 1, define the parameters $\gamma_i \in (0,1)$, $\varphi_i \in (0,1)$, $T_{i2} > 0$ of the function as ϑ_i, where T_{i2} is a prescribed-time constant and $c_i > 0$ is the parameter to be designed.

Theorem 2 For the follower model (8) considering external disturbances, under the controller (21) and adaptive law (20), the follower can achieve tracking of the leader within a preset time, forming and maintaining the predetermined formation.

Proof: Construct the Lyapunov candidate function as follows:

$$V_2 = \frac{1}{2} \boldsymbol{s}_i^T \boldsymbol{s}_i + \frac{1}{2\lambda_i} \tilde{\boldsymbol{l}}_i^T \tilde{\boldsymbol{l}}_i \tag{22}$$

Taking its time derivative yields:

$$\dot{V}_2 = \boldsymbol{s}_i^T \left[\boldsymbol{\Xi}_i + k_{i2} \left(-\alpha_{i0} \dot{\boldsymbol{p}}_0 + \sum_{k=0}^{m} \alpha_{ik} \left(\boldsymbol{w}_i + \boldsymbol{h}_i \boldsymbol{u}_i + \boldsymbol{l}_i \right) - \sum_{k=1}^{m} \alpha_{ik} \dot{\boldsymbol{v}}_i \right) \right] - \frac{1}{\lambda_i} \tilde{\boldsymbol{l}}_i^T \dot{\tilde{\boldsymbol{l}}}_i \tag{23}$$

Substituting the controller (21) into (23) yields:

$$\begin{aligned} \dot{V}_2 &= \boldsymbol{s}_i^T \left[-\frac{1}{2} c_i \vartheta_i \boldsymbol{s}_i + k_{i2} \sum_{k=0}^{m} \alpha_{ik} \tilde{\boldsymbol{l}}_i \right] - \frac{1}{\lambda_i} \tilde{\boldsymbol{l}}_i^T \dot{\hat{\boldsymbol{l}}}_i \\ &= -\frac{1}{2} c_i \vartheta_i \boldsymbol{s}_i^T \boldsymbol{s}_i + \tilde{\boldsymbol{l}}_i^T \left(k_{i2} \sum_{k=0}^{m} \alpha_{ik} \boldsymbol{s}_i - \frac{1}{\lambda_i} \dot{\hat{\boldsymbol{l}}}_i \right) \end{aligned} \tag{24}$$

Substituting the adaptive law (20) into (24) yields:

$$\begin{aligned} \dot{V}_2 &= -\frac{1}{2} c_i \vartheta_i \boldsymbol{s}_i^T \boldsymbol{s}_i + \tilde{\boldsymbol{l}}_i^T \left(k_{i2} \sum_{k=0}^{m} \alpha_{ik} \boldsymbol{s}_i - \frac{1}{\lambda_i} \dot{\hat{\boldsymbol{l}}}_i \right) \\ &= -\frac{1}{2} c_i \vartheta_i \boldsymbol{s}_i^T \boldsymbol{s}_i + \frac{1}{2\lambda_i} c_i \vartheta_i \tilde{\boldsymbol{l}}_i^T \hat{\boldsymbol{l}}_i \\ &\le -\frac{1}{2} c_i \vartheta_i \boldsymbol{s}_i^T \boldsymbol{s}_i - \frac{1}{2\lambda_i} c_i \vartheta_i \tilde{\boldsymbol{l}}_i^T \tilde{\boldsymbol{l}}_i + \frac{1}{2\lambda_i} c_i \vartheta_i \boldsymbol{l}_i^T \boldsymbol{l}_i \\ &\le -c_i \vartheta_i V_i + \zeta_i \end{aligned} \tag{25}$$

where $c_i > 0$, $\zeta_i = c_i \vartheta_i \boldsymbol{l}_i^T \boldsymbol{l}_i / (2\lambda_i)$. By Assumption 2, $\boldsymbol{l}_i$ is bounded, which implies that ζ_i is bounded. Then, by Lemma 1, the formation error converges to the set $\mathrm{E}_i = \max\{\mathrm{E}_{i1}, \mathrm{E}_{i2}\}$ within the prescribed-time $T_a = T_{i1} + T_{i2}$.

$$\mathrm{E}_{i1} = \left\{ \boldsymbol{x} : V(\boldsymbol{x}) \le V(0) e^{-\frac{c_i T_{i2} \varphi_i}{\gamma_i (1+\varphi_i)}} + \frac{\zeta_i \gamma_i T_{i2} / (c_i \varphi_i)}{\sqrt{T_{i2}^2 / 4 + \gamma_i T_{i2} / (c_i \varphi_i)}} \ln \left(\frac{\sqrt{T_{i2}^2 / 4 + \gamma_i T_{i2} / (c_i \varphi_i)} + T_{i2} / 2}{\sqrt{T_{i2}^2 / 4 + \gamma_i T_{i2} / (c_i \varphi_i)} - T_{i2} / 2} \right) \right\} \tag{26}$$

$$\mathrm{E}_{i2} = \left\{ \boldsymbol{x} : V(\boldsymbol{x}) \le \frac{\gamma_i \zeta_i}{c_i} + \left(V(\boldsymbol{x}(T_{i2})) - \frac{\gamma_i \zeta_i}{c_i} \right) e^{-\frac{c_i}{\gamma_i} (t - T_{i2})} \right\} \tag{27}$$

Thus, theorem 2 holds.

4. Simulation

In this section, numerical simulation results are presented to verify the effectiveness of the proposed control strategy. All simulations are conducted using MATLAB/Simulink 2024b with a fixed step size of 1ms. The formation consists of one virtual leader (indexed by 0) and three followers (indexed by 1, 2, and 3). The communication topology is shown in Figure. 1.

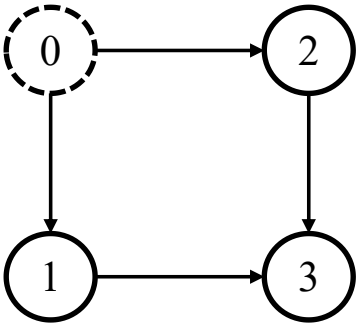


Figure.1 Communication network of the formation

4.1 Parameter Setting

The mass of each STR-UAV is 1.2kg. The initial states of the formation members are given as: $\boldsymbol{p}_1=[-1,22,0]^T$, $\boldsymbol{p}_2=[4,19,0]^T$, $\boldsymbol{p}_3=[3,23,0]^T$, $\boldsymbol{v}_1=\boldsymbol{v}_2=\boldsymbol{v}_3=[0,0,0]^T$. The state information of the virtual leader is: $\boldsymbol{p}_0=[0,20,3]^T$, $\boldsymbol{v}_0=[1.5,-6\sin(0.3t),0.8]^T$. The controller parameters are set as: $k_{i1}=0.8$, $k_{i2}=0.4$, $a_i=0.7$, $T_1=5$, $T_2=0.01$, $c_i=2$. The desired position offsets for the formation are: $\boldsymbol{p}_{1d}=[-3,0,-3]^T$, $\boldsymbol{p}_{2d}=[3,0,-3]^T$, $\boldsymbol{p}_{3d}=[0,0,-6]^T$. The external disturbances are set as: $\boldsymbol{l}_{is}=[0.1\sin(t),0.1\cos(0.5t),0.1\sin(t+0.2)]^T\,\mathrm{m/s^2}$. In addition, Table 1 presents the relevant information on the actuator faults of the followers.

Table 1 Failure information for STR-UAV formation members

STR-UAV	Fault Time t_{id}	$\boldsymbol{\omega}_i(t)$	$\boldsymbol{h}_i(t)$
Follower 1	$t_{1d}=10\mathrm{s}$	$diag\left(0.5+0.5e^{-10\max\{0,t-t_{1d}\}},1,1\right)$	$[5\left(1-e^{-10\max\{0,t-t_{3d}\}}\right),0,0]^T$
Follower 2	$t_{2d}=15\mathrm{s}$	$diag\left(1,0.8+0.2e^{-10\max\{0,t-t_{2d}\}},1\right)$	$[0,2\left(1-e^{-10\max\{0,t-t_{2d}\}}\right),0]^T$
Follower 3	$t_{3d}=20\mathrm{s}$	$diag\left(1,1,0.9+0.1e^{-10\max\{0,t-t_{3d}\}}\right)$	$[0,0,2\left(1-e^{-10\max\{0,t-t_{3d}\}}\right)]^T$

4.2 Simulated Analysis

According to the information in Table 1, followers 1, 2, and 3 experience actuator faults at 10 s, 15 s, and 20 s, respectively. Figures. 2-7 present the simulation results of the adaptive practical prescribed-time fault-tolerant control strategy proposed in this paper, which accounts for external disturbances and actuator faults.

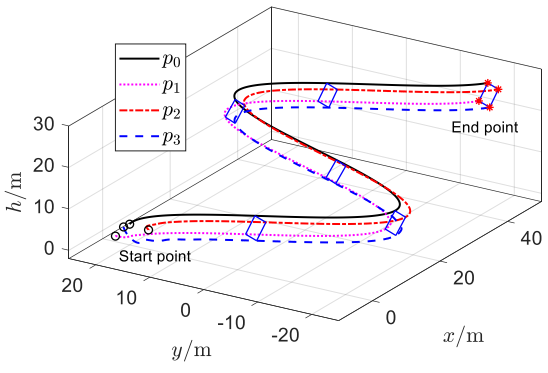


Figure.2 - Flight path

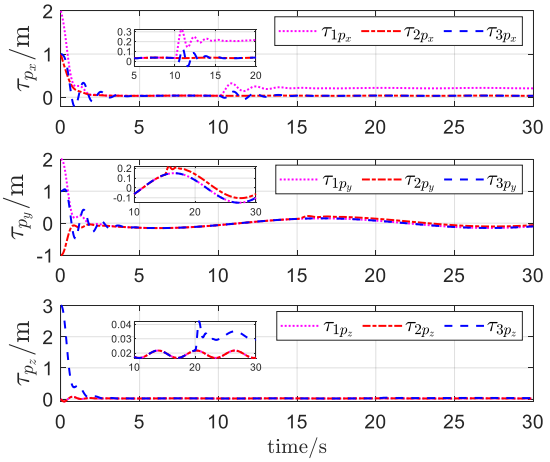


Figure.3 - Position errors

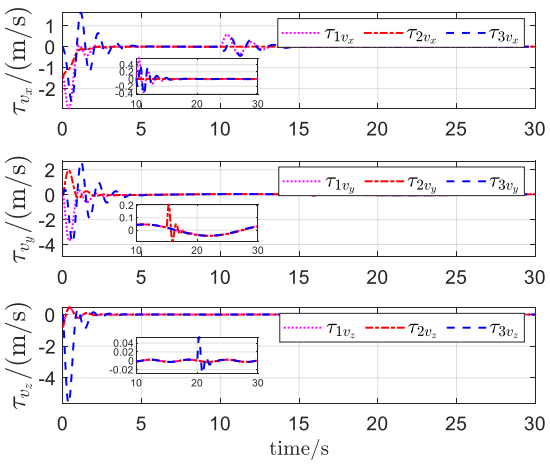


Figure.4 - Velocity errors

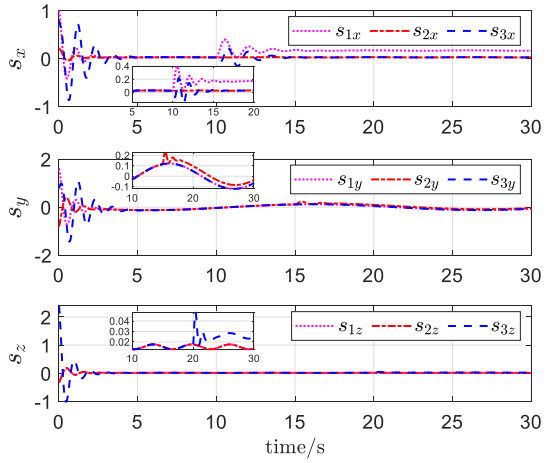


Figure.5 - Sliding mode surfaces

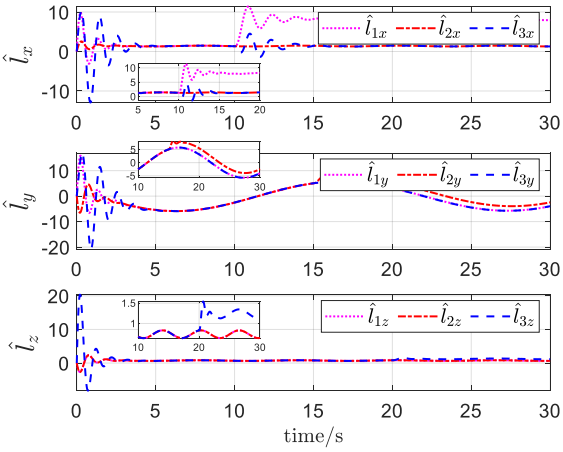


Figure.6 - Disturbance estimates

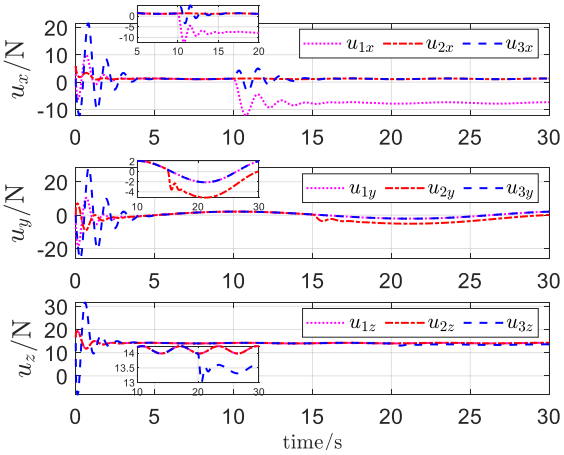


Figure.7 - Control inputs

Figure. 2 shows the trajectory of the STR-UAV formation. It can be observed that under the proposed control strategy, the formation can still form the desired configuration within the prescribed time even in the presence of external disturbances and sudden actuator faults, which verifies the effectiveness of the proposed control strategy. Figures. 3, 4 and 5 present the convergence curves of the position errors, velocity errors and prescribed-time sliding mode surface, respectively. It can be seen from the figures that both the errors and the sliding mode surface converge to the neighborhood of the origin within the prescribed time. Moreover, they can quickly reconverge after the transient peaks induced by sudden faults, which further validates the fault tolerance and robustness of the proposed control strategy. Figures. 6 and 7 show the curves of the adaptive parameters and control inputs, respectively, verifying their boundedness.

5. Conclusion

This paper proposes an adaptive prescribed-time fault-tolerant control strategy for STR-UAV formations considering external disturbances and actuator faults, achieving stable control within a predetermined timeframe. A novel prescribed-time sliding mode surface ensures stable convergence within the prescribed time, independent of initial conditions. Combined with a prescribed-time adaptive law, it enables precise estimation of unknown disturbances and actuator effectiveness faults, ultimately unifying formation timeliness with disturbance robustness and fault tolerance. This strategy provides a viable technical solution for STR-UAV formations operating in complex disturbed environments, expanding the application scenarios of prescribed-time control and adaptive methods to fault-tolerant formation control systems. Future research can focus on areas such as multi-disturbance coupling, actuator failure accommodation and heterogeneous aircraft coordination.

6. Declaration of Competing Interest

The authors declare that they have no known competing financial interests or personal relationships that could have appeared to influence the work reported in this paper.

7. Acknowledgements

This work was supported by the National Natural Science Foundation of China (Grant No. 62273277).

8. Contact Author Email Address

Xiaolu Li: lixiaolu@mail.nwpu.edu.cn

Changqing Wang: wangcq@nwpu.edu.cn

Yong Guo: guoyong@nwpu.edu.cn

Aijun Li: liaijun@nwpu.edu.cn

9. Copyright Statement

The authors confirm that they, and/or their company or organization, hold copyright on all of the original material included in this paper. The authors also confirm that they have obtained permission, from the copyright holder of any third party material included in this paper, to publish it as part of their paper. The authors confirm that they give permission, or have obtained permission from the copyright holder of this paper, for the publication and distribution of this paper as part of the ICAS proceedings or as individual off-prints from the proceedings.

References

[1] Sabour M, Jafary P, and Nematiyan S. Applications and classifications of unmanned aerial vehicles: A literature review with focus on multi-rotors. The Aeronautical Journal, Vol. 127 No. 1309, pp 466-490, 2023.

[2] Lyu M, Zhao Y, Huang C, and Huang H. Unmanned aerial vehicles for search and rescue: A survey. Remote Sensing, Vol. 15 No. 13, pp 3266, 2023.

[3] Hoang M T O, Grøntved K A R, Van Berkel N, Skov M B, Christensen A L, and Merritt T. Drone swarms to support search and rescue operations: Opportunities and challenges. Cultural Robotics: Social Robots and Their Emergent Cultural Ecologies, 2023: 163-176.

[4] Li X, Wang C, Guo Y, and Li A. Disturbance Observer-based Distributed Practical Prescribed-Time Formation Tracking Control for Small Tandem-rotor UAVs Accounting for Actuator Dynamics. Aerospace Science and Technology, Vol. 177, pp 112340, 2026.

[5] Li X, Wang C, Guo Y, and Li A. Dynamic surface-based distributed practical predefined-time cooperative control for flight formation of a novel small tandem-rotor wheeled UAV. ISA transactions, Vol. 167, pp 575-588, 2025.

[6] Sun Y, Guo Y, and Li A. Formation Control and Experiment for Propeller‐Driven Car‐Like Robots with Amplitude and Rate Saturation Under Steering Fault‐Tolerant Control. Journal of Field Robotics, Vol. 43, No. 3, pp 1568-1590, 2026.

[7] Sun Y, Guo Y, and Li A. Tracking Control and Experiment for Propeller‐Driven Wall‐Climbing Robot Considering Actuator Dynamics and Saturation. Journal of Field Robotics, Vol. 42, No. 8 pp 4115-4132, 2025.

[8] Ouyang Q, Wu Z, Cong Y, and Wang Z. Formation control of unmanned aerial vehicle swarms: A comprehensive review. Asian Journal of Control, Vol. 25, No. 1, pp 570-593, 2023.

[9] Yang Y, Xiong X, and Yan Y. UAV formation trajectory planning algorithms: A review. Drones, Vol. 7, No. 1 pp 62, 2023.

[10] Liu H, Li B, and Ahn C K. Asymptotically stable learning-based formation control for multi-quadrotor UAVs. IEEE Internet of Things Journal, Vol. 12, No. 13, pp 24985-24995, 2025.

[11] Ding C, Zhang Z, Miao Z, and Wang Y. Event-based finite-time formation tracking control for UAV with bearing measurements. IEEE Transactions on Industrial Electronics, Vol. 72, No. 7, pp 7482-7492, 2024.

[12] Miao Q, Zhang K, and Jiang B. Fixed-time collision-free fault-tolerant formation control of multi-UAVs under actuator faults. IEEE Transactions on Cybernetics, Vol. 54, No. 6, pp 3679-3691, 2024.

[13] Zeng D, Cai C, Liu Y, Zhao J, and Li C. Practical prescribed-time control for underactuated marine surface vessels: Theory and experiment. IEEE Transactions on Automation Science and Engineering, Vol. 22, pp 14074-14083, 2025.

[14] Jia T, Yan H, Zhang H, Li H, and Zhang Y. Adaptive anti-disturbance performance guaranteed formation tracking control for quadrotor UAVs via aperiodic signal updating. IEEE Transactions on Systems, Man, and Cybernetics: Systems, Vol. 54, No. 9, pp 5212-5223, 2024.

[15] Ma Z, Gong H, and Wang X. Formation fault-tolerant control for multiple UAVs with external disturbances. Aircraft Engineering and Aerospace Technology, Vol. 96, No. 3, pp 403-416, 2024.

[16] Yin T, Gu Z, and Xie X. Observer-based event-triggered sliding mode control for secure formation tracking of multi-UAV systems. IEEE Transactions on Network Science and Engineering, Vol. 10, No. 2, pp 887-898, 2022.

[17] Xu L, Wang Y, Wang X, and Peng C. Distributed active disturbance rejection formation tracking control for

quadrotor UAVs. IEEE Transactions on Cybernetics, Vol. 54, No. 8, pp 4678-4689, 2023.

[18]Zhang J, Zhang P, and Yan J. Distributed adaptive finite-time compensation control for UAV swarm with uncertain disturbances. IEEE Transactions on Circuits and Systems I: Regular Papers, Vol. 68, No. 2, pp 829-841, 2020.

[19]Wang J, Liu J, Chen P, and Chen K. Distributed observer-based formation control for leader-follower multi-UAVs with collision avoidance. IEEE Transactions on Vehicular Technology, Vol. 74, No. 8, pp 11951-11962, 2025.

[20]Liu Z, Li J, Shen J, Wang X, and Chen P. Leader–follower UAVs formation control based on a deep Q-network collaborative framework. Scientific Reports, Vol. 14, No. 1, pp 4674, 2024.

[21]Liu Y, Liu Z, Wang G, Yan C, Wang X, and Huang Z. Flexible multi-UAV formation control via integrating deep reinforcement learning and affine transformations. Aerospace Science and Technology, Vol. 157, pp 109812, 2025.